Non-isothermal crystallization kinetics and morphology of poly(3-hydroxybutyrate)/pluronic blends

Moira Ambrosi[a*], Martina Raudino[a], Isabel Diañez[b], Inmaculada Martínez[b]

[a]Department of Chemistry and CSGI, University of Florence, Via della Lastruccia 3-13, 50019 Sesto Fiorentino, Florence, Italy

[b]Department of Chemical Engineering, Chemical Process and Product Technology Research Center (Pro2TecS), University of Huelva, Campus El Carmen, 21071 Huelva, Spain

Corresponding Author

*Moira Ambrosi. Email: moira.ambrosi@unifi.it; phone: +390554573018.

Keywords

Biopolymer blends; Non-isothermal crystallization; Morphology; Rheology; Differential Scanning Calorimetry; X-ray Scattering.

Abstract

Poly(3-hydroxybutyrate), PHB, was mixed with pluronic F68 or F127 to obtain polymer blends with increased hydrophilicity and thus suitable for biomedical applications. Blend films were obtained by thermomoulding keeping the pluronic content ≤ 17 wt% to avoid immiscibility. The non-isothermal crystallization kinetics of the blends was investigated by both differential scanning calorimetry (DSC) and rheology. PHB and pluronics were found to be miscible in the melt with both pluronics acting as diluent. Polarized optical microscopy (POM) and X-ray scattering (SAXS and WAXS) revealed that blending increased the overall crystallinity, promoting crystal ordering through the formation of more resolved, ring-banded spherulites. However, the different diffusion rate of pluronic F68 and F127 led to a different segregation extent of pluronic in the extralamellar domains with different final morphological homogeneity. The mechanical properties of the blends intimately correlated with the structure at the nano and microscale.

1. Introduction

Biopolymers are receiving increasing attention as they represent a valid alternative to petroleum-based counterparts in several fields, such as manufacturing, household, and medicine, where they are used to develop implantable biomaterials and drug-delivery

systems [1–4]. Poly(3-hydroxybutyrate) (PHB), a biodegradable semicrystalline polyester produced via biosynthesis by bacterial fermentation [5,6], is one of the most promising biopolymers. Due to its biocompatibility, processability and degradability, PHB shows great potential to produce biomedical materials such as controlled release devices [7–9], wound dressing materials and scaffolds for tissue engineering [10,11]. However, the highly hydrophobic nature of PHB limits its application. Indeed, drug release from PHB matrices is mainly achieved through the dissolution of drug present on the spherulite surface or located in the spherulite-spherulite boundaries, followed by a slower release through water penetration and the formation of channels and pores. The mass loss due to surface erosion appears not to play any significant role in the active release process, being almost negligible when compared to other bulk-degrading blends as poly(lactide-glycolide) systems [12]. Therefore, the efficient application of PHB-based materials as drug delivery devices depends on the formulation of suitable blends with other biocompatible polymers which could fast the degradation process. Consequently, PHB has been blended with several rather hydrophilic polymers, as PEO [13,14] and pluronics [15,16], in order to increase its water wettability, swelling properties and mechanical behavior. The presence of another component affects the PHB crystalline structure, thus changing the mechanism and rate of degradation, the drug compatibility and drug diffusion [12]. The drug release profile has been proved to be strongly influenced by blend composition and morphology, in particular with respect to the presence of nano- and micro-pores and channels [17]. It is therefore clear that tailored biomedical devices can be accurately designed by a thorough control of the fabrication conditions.

In the present work, binary blends of PHB and pluronic F68 or pluronic F127 were prepared by thermomoulding. Pluronics are linear triblock copolymers approved for

medical use by FDA consisting of a central polypropylene glycol (PPO) hydrophobic block and two external hydrophilic polyethylene oxide (PEO) segments. F68 and F127 differ by the length of PPO and PEO blocks with F68 being slightly more hydrophilic than F127 (HLB = 29 and 22, respectively). Based on previous experiments conducted on similar PHB/PEO blends [18] and on our results on PHB/F127 systems, the pluronic content was kept low enough (≤ 17 wt%) to avoid immiscibility.

The final morphology was investigated by polarized optical microscopy (POM) and small- and wide-angle X-ray scattering (SAXS, WAXS) to assess whether and how the presence of pluronic influenced the crystalline structure of PHB. Several efforts have been made in the past to clarify how the crystallization kinetics and the final morphology of the crystalline component are influenced by other blend constituents both in the case of crystalline/crystalline and amorphous/crystalline polymer blends [19–22]. For PHB-based blends, melt crystallization was found to produce a broad range of structures with different degree of segregation depending on the fabrication conditions, the polymer/polymer interaction strength and the supermolecular structure of spherulites formed by the high temperature crystallizing PHB [13,14,23,24]. In the present work, blending was found to increase the crystallinity and to promote crystal ordering with formation of more resolved spherulites. Addition of a low amount of pluronics (5 wt%) induced the formation of rather homogeneous blends mostly containing double-banded spherulites with constant twist period. The different diffusion rate of F68 and F127 affected the final structure that became more ordered in the presence of F68, i.e. the diluent with the highest diffusivity. Furthermore, the morphology distribution increased by increasing the pluronic content.

The crystallization kinetics in non-isothermal conditions was investigated by calorimetric (differential scanning calorimetry, DSC) and rheological measurements.

To the best of our knowledge, the study of the non-isothermal melt crystallization of PHB/pluronic blends has never been reported. Furthermore, only a few reports refer to the use of rheology as a suitable technique to follow polymer blends' crystallization [25–29]. The combined use of DSC and rheology was particularly useful. Indeed, the two techniques were found to give analogous results being complementary at the same time. While DSC provided the crystallization rate parameters and the final degree of crystallinity, rheometry allowed investigating the overall process including the induction period before the crystals' occurrence which is not accessible by calorimetric experiments. Our results suggest that both pluronics acted as diluents retarding PHB crystallization.

Finally, the effect of blending on the final mechanical properties of the systems was investigated as well. Blends were all found to possess higher Young's modulus and lower elongation at break as compared to neat PHB. The high crystallinity observed for all blend compositions, possibly combined with their heterogeneous morphology, could explain the variation of mechanical performances observed upon blending.

From a fundamental point of view, our results contribute to disclose the crystallization process for crystalline/crystalline polymer blends that have received less attention than fully amorphous and amorphous/crystalline systems. Moreover, our study shows the potentiality of rheometry as a tool to investigate all stages of polymer crystallization. The obtained results are helpful to correlate the structure and properties of polymers processed in dynamic, non-isothermal conditions [30].

2. Experimental Section

2.1 Materials

Poly(3-hydroxybutyrate) (PHB) pellets with the trade name Mirel M2100 were purchased from Metabolix, Inc. (USA) with a molecular weight $M_w = 3.7 \cdot 10^5$ g·mol^{-1} and polydispersity index (M_w/M_n) in the range 1.60 ÷ 1.85.

Pluronic F68 (M_w = 8400) and pluronic F127 (M_w = 12600) were supplied by Sigma-Aldrich (Italy). All reagents were used as received.

2.2 Films preparation

PHB pellets were first ground using an IKA-Werke model MF10 basic microfine grinder (IKA-Werke GmbH & Co.KG, Germany) operating at 3000 rpm to obtain a better pre-mixing with pluronics. PHB/pluronic mixtures were pre-mixed manually and then molded by compression using a 25T hot plate press (MTI Corporation, Richmond, USA) at 190 ºC and 50 kN gauge pressure for 1 min followed by 3 min at 100 kN in order to obtain films of about 300 μm in thickness.

The prepared samples will be referred as: PHB (pure polymer), F68-5 (PHB/F68 blend containing 5 wt% of pluronic F68), F68-17 (PHB/F68 blend containing 17 wt% of pluronic F68), F127-5 (PHB/F127 blend containing 5 wt% of pluronic F127) and F127-17 (PHB/F127 blend containing 17 wt% of pluronic F127).

All the experiments listed below were performed on samples one week after their preparation. Meanwhile, samples were kept at room temperature.

2.3 Differential scanning calorimetry (DSC)

Calorimetric measurements were carried out by means of a Q1000 Differential Scanning Calorimeter (TA Instruments). 3 mg of the films were placed in hermetic aluminum pans, which were sealed under nitrogen atmosphere. The samples were first heated at 190 °C at a heating rate of 20 °C/min and kept at this temperature for 10 min to melt and homogenize the material and to erase its thermal history [31]. They were then cooled at 30 °C with a cooling rate of 5 °C/min and heated again at 190 °C with a

heating rate of 20 °C/min. The reported melting points, T_m, were taken as the temperature of the endothermic peak for the second heating run. The associated enthalpy change, ΔH_m, was determined by integrating the heat flow curve. The glass transition temperatures, T_g, were determined by first heating the samples at 190 °C for 10 min, cooling them at -90 °C at 10 °C/min and heating them again at 190 °C. T_g was determined as the middle point of the transition during the second heating run at 20 °C/min. The degree of crystallinity, X_c, was obtained from the melting peak recorded during the second heating run as follows:

$$\mathrm{X_c} = \frac{\Delta \mathrm{H_m}}{\mathrm{w}\Delta \mathrm{H_f^0}} \cdot 100 \qquad (1)$$

where ΔH_m is the melting enthalpy of the sample ($J \cdot g^{-1}$), w is the weight fraction of PHB in the blend film and ΔH_f^0 is the heat of fusion of 100% crystalline PHB which is assumed to be 146 $J \cdot g^{-1}$[16].

The crystallization behavior of PHB and PHB/pluronic blends was investigated by analyzing the corresponding non-isothermal crystallization kinetics. The relative crystallinity, X_t, as a function of time t, can be expressed as follows:

$$\mathrm{X_t} = \frac{\int_0^{\mathrm{t}} \left(\frac{\mathrm{dH_c}}{\mathrm{dt}}\right) \mathrm{dt}}{\int_0^{\infty} \left(\frac{\mathrm{dH_c}}{\mathrm{dt}}\right) \mathrm{dt}} \qquad (2)$$

where dH_c is the crystallization enthalpy released in an infinitesimal time range dt.

The relationship between the crystallization time t and the crystallization temperature T is:

$$\mathrm{t} = \frac{\mathrm{T_o} - \mathrm{T}}{\phi} \qquad (3)$$

where Φ is the cooling rate, T_0 is the initial crystallization temperature, and T is the crystallization temperature at time t.

Avrami equation is often used to describe the isothermal crystallization kinetics; the behavior of X_t versus time is expressed as:

$$X_t = 1 - \exp(-k_a t^n) \qquad (4)$$

where n is the Avrami exponent depending on the crystallization mechanism, k_a is the overall rate constant related both nucleation and growth rate parameters and t is the time form the start of phase transformation [32–34].

Equation (4) can be rewritten as follows:

$$\log[-\ln(1 - X_t)] = \log k_a + n\log t \qquad (5)$$

A plot $\log[-\ln(1 - X_t)]$ versus $\log t$ would give a straight line from which both k_a and n can be derived from the intercept and the slope, respectively.

Considering the non-isothermal character of the crystallization process in the present work, the k_a value was corrected by the cooling rate ϕ according to Jeziorny [35]. Assuming constant the cooling rate, the final form of the rate constant k_c is given by equation (6):

$$\log k_c = \frac{\log k_a}{\phi} \qquad (6)$$

By knowing n and k_c, the half-time of crystallization, defined as the time needed to achieve 50% of the final crystallinity, can be obtained by equation (7) [36]:

$$t_{\frac{1}{2}} = \left(\frac{\ln 2}{k_c}\right)^{\frac{1}{n}} \qquad (7)$$

2.4 Rheological measurements

Polymer disks of 2.5 cm diameter and 1 ± 0.3 mm thickness were obtained from 8 g of material by compression molding between two metallic and silicon sheets in a hot plate press (25T, MTI Corporation, Richmond, USA). The polymer was melted at 190 °C for 3 min without pressurizing the sample and, after molding, it was cooled at room temperature.

Rheological measurements were performed using a controlled-stress rheometer Physica MCR501 (Anton Paar Germany GmbH, Ostfildern, Germany) equipped with 25 mm parallel plate-plate geometry and using a gap thickness of 0.5 mm. The non-isothermal crystallization kinetics were monitored by evaluating the storage and loss moduli (G' and G'') and the complex viscosity η^* as a function of time. Samples were first heated to 190 °C, equilibrated at this temperature for 10 min and then downward temperature ramps of 5 ºC/min were applied from 190 to 30 ºC. The experiments were carried out in oscillatory mode, time sweep test at the frequency of 1 Hz and constant stress of 100 Pa. To ensure a correct stress control, stress sweep tests were previously performed on the different samples and both at 30 and 190 ºC in order to perform measurements within the linear viscoelastic regime.

2.5 Polarized optical microscopy (POM)

Polarized optical microscopy images were acquired by means of a Leica ICC50 W optical microscope equipped with a pair of crossed polarizers, coupled with a Linkam 420 Heating-Freezing Stage by Linkam Scientific Instruments. In order to assess the final morphology and its evolution during the non-isothermal conditions used for both DSC and rheology, thin layers of PHB and its blends with pluronics (about 300 □m) were placed between glass microscope slides, heated at 190 °C for 10 min to erase their thermal history and then cooled to 30 °C with a gradient of 5 °C/min.

2.6 Small- and wide-angle X-ray scattering (SAXS-WAXS)

SAXS-WAXS measurements were performed on as-prepared PHB and blend films by a HECUS S3-MICRO camera (Kratky-type) equipped with two position-sensitive detectors (OED 50m) containing 1024 channels of 54 μm in width. Cu K_α radiation (λ = 1.542 Å) was provided by an ultrabrilliant point microfocus X-ray source (GENIX-Fox 3D, Xenocs, Grenoble), operating at a maximum power of 50 W. The sample-to-detector distance was 281 mm. The volume between the sample and detector was kept under vacuum during the measurements to minimize the scattering from the air. The Kratky camera was calibrated in the small angle region by using silver behenate (58.34 Å) [37], whereas lupolen (4.12 and 3.8 Å) was used as a reference for the wide-angle region. SAXS curves were obtained in the scattering vector, q, range between 0.01 and 0.54 $Å^{-1}$, with $q = \frac{4\pi}{\lambda}\sin\theta$ where θ is the scattering angle. The investigated WAXS region ranged from 1.3 to 1.9 $Å^{-1}$.

Samples were analyzed at 25 °C by using a demountable 1 mm cell having the blend films as windows. All scattering curves were corrected for the empty-cell contribution by considering the relative transmission factor. The intensity profiles were corrected by subtracting the background intensity associated with thermal density fluctuation I_{fl} according to the Porod-Ruland model [38]:

$$I(q) = K_p \frac{\exp(-\sigma^2 q^2)}{q^4} + I_{fl} \qquad (8)$$

where K_p is the Porod constant, σ is a parameter related to the thickness of crystal/amorphous interphase, and I_{fl} is the background intensity to subtract from SAXS curves. The values of these parameters were obtained from the curve fitting in the high-q region (0.1-0.16 $Å^{-1}$).

The long period or interlamellar spacing (LP) of the sample was determined from the Lorentz-corrected plot $I(q)q^2$ versus q as $LP = 2\pi/q^*$, where q^* is the peak value found in the Lorentz-corrected plot corresponding to the first order of the crystalline repeat in the spherulite.

In the lamellar stack model with sharp phase boundary, the long period LP represents the sum of the crystal thickness (l_c) and the amorphous layer thickness (l_a). The average long period, the amorphous thickness, and the crystal thickness can all be obtained from SAXS measurements by calculating the one-dimensional correlation function γ(z) [39]. The one-dimensional correlation function was calculated by using SasView 4.1.2 software.

2.7 Tensile properties

Tensile tests were carried out by using a Shimadzu AG-IS testing machine (Shimadzu Corporation, Kyoto, Japan). Test specimens for tensile tests according to UNI-EN ISO 527-3 standard were obtained from the films by means of a die cutting machine (ATS Faar, S.p.A, Milan, Italy). Dumb-bell specimens type 5 (6 ± 0.5, 33 ± 0.5 and 2 ± 0.5 mm of width, length and thickener of narrow section, respectively) were tested at room temperature by following the UNE-EN ISO 527-3 standard with a crosshead speed of 50 mm/min and a load cell bob 1kN. Average Young's Modulus, tensile strength and strain at break were calculated from the resulting stress-strain curves as the average of five measurements on each sample.

3. Results and Discussion

3.1 Thermal behavior of PHB and PHB/pluronic blends

The thermal behavior of PHB, pluronics F68 and F127 and PHB/pluronic blend films was investigated by DSC. The melting points, T_m, the corresponding enthalpy of fusion, ΔH_m, the glass transition temperatures, T_g, and the degree of crystallinity, X_c, determined by means of equation (1) are reported in Table 1.

All blend compositions showed a single T_m value, ascribable to the melting of crystalline PHB. The small T_m depressions recorded for all blends suggested that PHB and the used pluronic were weakly interacting polymers [40]. For the investigated composition range, both pluronics appeared to be miscible with PHB in the amorphous state as evidenced by the presence of a single T_g value.

Table 1. Melting points, T_m, enthalpies of fusion, ΔH_m, glass transition temperatures, T_g, and degrees of crystallinity, X_c, determined by DSC measurements for all the investigated samples. X_c values for F68 and F127 were obtained from X-ray diffractometry (XRD).

Sample	T_m (°C) ± 1%	ΔH_m (J·g$_{PHB}^{-1}$) ± 5%	T_g (°C) ± 5%	X_c % ± 5%
PHB	162.4	46.9	0.39	32.1
F68-5	161.3	62.2	-7.5	42.6
F68-17	160.3	60.9	-9.3	41.7
F127-5	160.6	54.2	-5.2	37.1
F127-17	159.2	49.6	-10.0	34.0
F68	53.0	116.2	-62.4	73*
F127	53.3	117.2	-64.4	77*

Although only two compositions were analyzed for each PHB/pluronic system, small negative deviations from the linear trend of T_g versus composition were recorded for the samples containing 5% of both F68 and F127 (see SI, Figure S1), which may be related to conformational entropic effects usually ascribed to a weakening of the interactions between chain segments of the stiffer component (PHB) due to the effect of the relatively more flexible chains of pluronic [41].

All blend compositions showed higher X_c values than neat PHB indicating that crystallinity was enhanced upon blending, in agreement with results previously reported by Kajjari et al. for PHB/F127 microspheres [16]. The effect was larger for F68-containing specimens, for which X_c was about 42%, significantly higher than that measured for neat PHB (32.1%). F127-5 and F127-17 blends exhibited X_c values of 37% and 34%, respectively, both closer to the value for neat PHB.

No endothermal peak due to the melting of crystalline pluronics could be detected in the second heating ramp of the DSC profile, suggesting that F68 and F127 were completely prevented from crystallization under the conditions used to erase the sample thermal history. Nevertheless, it is worthwhile to note that the F127-17 blend was close to the unstable region of the phase diagram: the presence of a small endothermic peak at 53 °C ascribable to the melting of crystalline pluronic in the first heating ramp evidences the presence of some crystalline F127. The value of the corresponding enthalpy of fusion indicated that about 35% of the pluronic F127 added to PHB could crystallize during the thermomoulding of the blend. The melting peak of crystalline pluronic disappeared after erasing the sample thermal history (see Figure S2 in SI file).

3.2 Non-isothermal crystallization behavior by DSC

The non-isothermal crystallization behavior of neat PHB and its blends with pluronics was assessed by analyzing the DSC crystallization exothermic peaks and the

development of the corresponding relative crystallinity [42,43]. The crystallization peaks of neat PHB and of the prepared blend compositions are reported in Figure 1a. Figure 1b shows the dependence of the relative crystallinity, X_t, on the crystallization time, t. It must be noted that the absolute time, i.e. the time including the so-called induction period elapsed before crystallization started, is reported on X-axes. All X_t versus time curves show the characteristic sigmoidal shape ranging from 0 at the inception of the process to 1 at crystallization completion. Table 2 lists the crystallization temperature, T_c (the peak maximum), the onset temperature, T_0, the Avrami exponent, n, the constant rate, k_c, and the half-time, $t_{1/2}$, determined by the $\log[-\ln(1-X_t)]$ versus logt plot after subtraction of the induction time. Fittings were carried out in the X_t range 0.2 ÷ 0.8 to minimize the contributions from the beginning and the end of the crystallization.

PHB showed a double crystallization peak with two maxima centered at 60.8 and 77.5 °C. Double or multiple melting peaks have been previously reported for semi-crystalline polymers and usually related to melting, re-crystallization and re-melting during heating, the presence of more than one crystal modifications (polymorphism), of different morphologies (lamellar thickness, distribution, perfection or stability), the physical aging and/or relaxation of the rigid amorphous fraction, and the coexistence of species with different molecular weight [44,45]. The interpretation of the dual crystallization peak is beyond the scope of the present study; however, the presence of only one melting peak and the results from SAXS analysis (see below) exclude the occurrence of polymorphism and of lamellar stacks with different thickness. A possible explanation might rely on the presence of different crystalline microstructures that, once formed, have no time to melt, re-organize and crystallize again [46]. Measurements carried out at different cooling rates (0.5 ÷ 10 °C/min) all showed the

presence of crystallization multiple peaks that could not be avoided even setting the cooling rate as low as 0.5 °C/min. Moreover, the double peak was also present when PHB was first heated to a temperature larger than 192 °C in order to avoid self-seeding nucleation as suggested by Cretois et al. [46] and Di Lorenzo et al. [47]. It is worthwhile noting that POM images did not show any crystalline nuclei for samples kept at 190 °C for 10 minutes. The PHB used in the present study is significantly more amorphous than that used by the above mentioned authors. Thus, the amorphous component of PHB might hamper the formation of stable crystals.

Unlike PHB, all blend compositions exhibited one exothermic peak with a maximum temperature T_c lower than neat PHB (at least with respect to the first maximum at 77.5 °C). Within each PHB/pluronic series, T_c further slightly decreased by increasing the amount of pluronic. Similarly, the onset of crystallization was delayed upon blending, and T_0 further decreased by increasing the pluronic content. Therefore, both pluronic polymers seemed to act as diluent increasing PHB chain mobility and thus retarding its crystallization [48]. The retarding effect played by pluronic on PHB crystallization is also deducible from the shift towards higher absolute times observed for the X_t versus t curves determined for all blend compositions (Figure 1b).

The Avrami analysis of the non-isothermal crystallization behavior revealed that the effect of pluronic addition on the crystallization mechanism changed with changing the amount of pluronic in the blend. Interestingly, neat PHB and both blend compositions containing the largest amount of pluronic (F68-17 and F127-17) showed n values of about 3.00 in accordance with three-dimensional spherical growth with athermal nucleation [49]. F68-5 and F127-5, instead, possessed n values of 5.64 and 5.40, respectively, meaning that pluronic induced a remarkable variation of the nucleation mechanism and the crystal growth geometry in these specimens [50]. Values for the

Avrami exponent above 5 are consistent with three-dimensional solid sheaf growth and athermal nucleation [51].

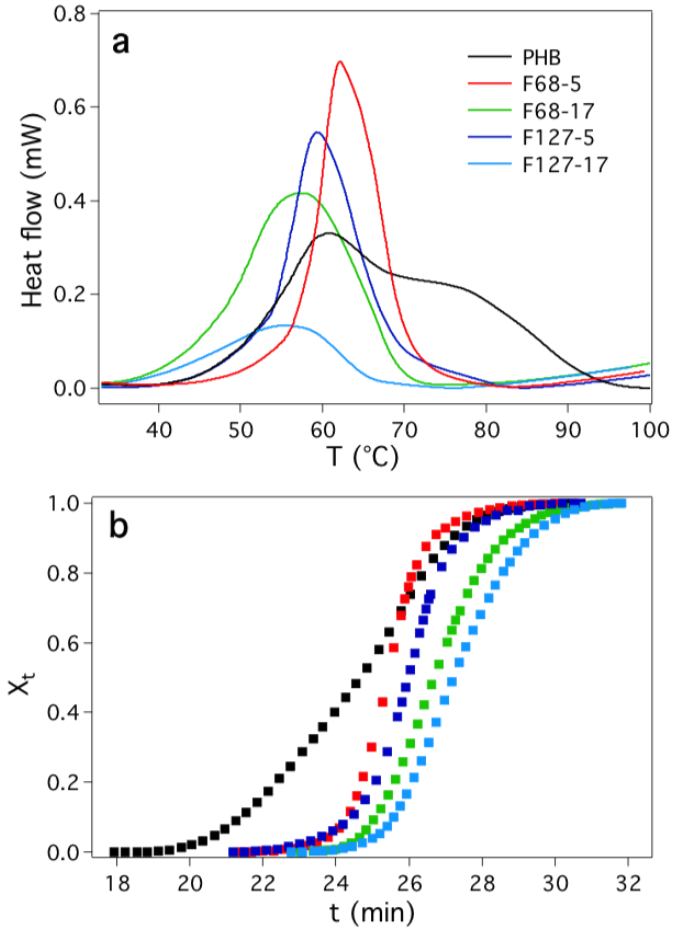

Figure 1. (a) Crystallization exothermic peaks and (b) development of relative crystallinity, X_t, as a function of absolute time for PHB and blend compositions.

Since k_c quite depends on n, k_c values obtained for processes featured by different n (i.e. different crystallization mechanism) cannot be directly compared [52]; therefore, the results obtained for the different specimens were more accurately discussed in term of $t_{1/2}$ (see Table 2). Neat PHB crystallization showed the lowest induction time and the highest $t_{1/2}$ in accordance with the position and shape of the crystallization exotherm. Indeed, crystallization of neat PHB is a complex process that spans over a

wide range of temperature. Concerning the blend compositions, the slight decrease of $t_{1/2}$ values observed within each set of samples with increasing the amount of pluronic agreed with the slight increase of undercooling ΔT determined for the blends containing 17% of pluronic (samples F68-17 and F127-17) possibly associated with a slight increase of the crystal growth rate.

Table 2. Crystallization temperature, T_c, onset temperature, T_0, Avrami exponent, n, constant rate, k_c, and half-time, $t_{1/2}$ for neat PHB and all blend compositions.

Sample	T_c (°C)	T_0 (°C)	n	k_c ×10 (min^{-n})	$t_{1/2}$ (min)
PHB	60.8 - 77.5	100.2	2.96	3.03	1.32
F68-5	62.1	82.9	5.64	1.94	1.25
F68-17	58.0	74.9	3.07	4.17	1.18
F127-5	59.2	84.1	5.40	1.71	1.29
F127-17	55.2	76.1	3.20	3.25	1.24

3.3 Morphology of blends by POM

The final morphology of PHB and PHB/pluronic blends and its evolution during the non-isothermal crystallization process was investigated by polarizing optical microscopy. Figure 2 shows POM images at the same magnification (5× - left and 20× - right) and temperature (30 °C) for all the investigated samples.

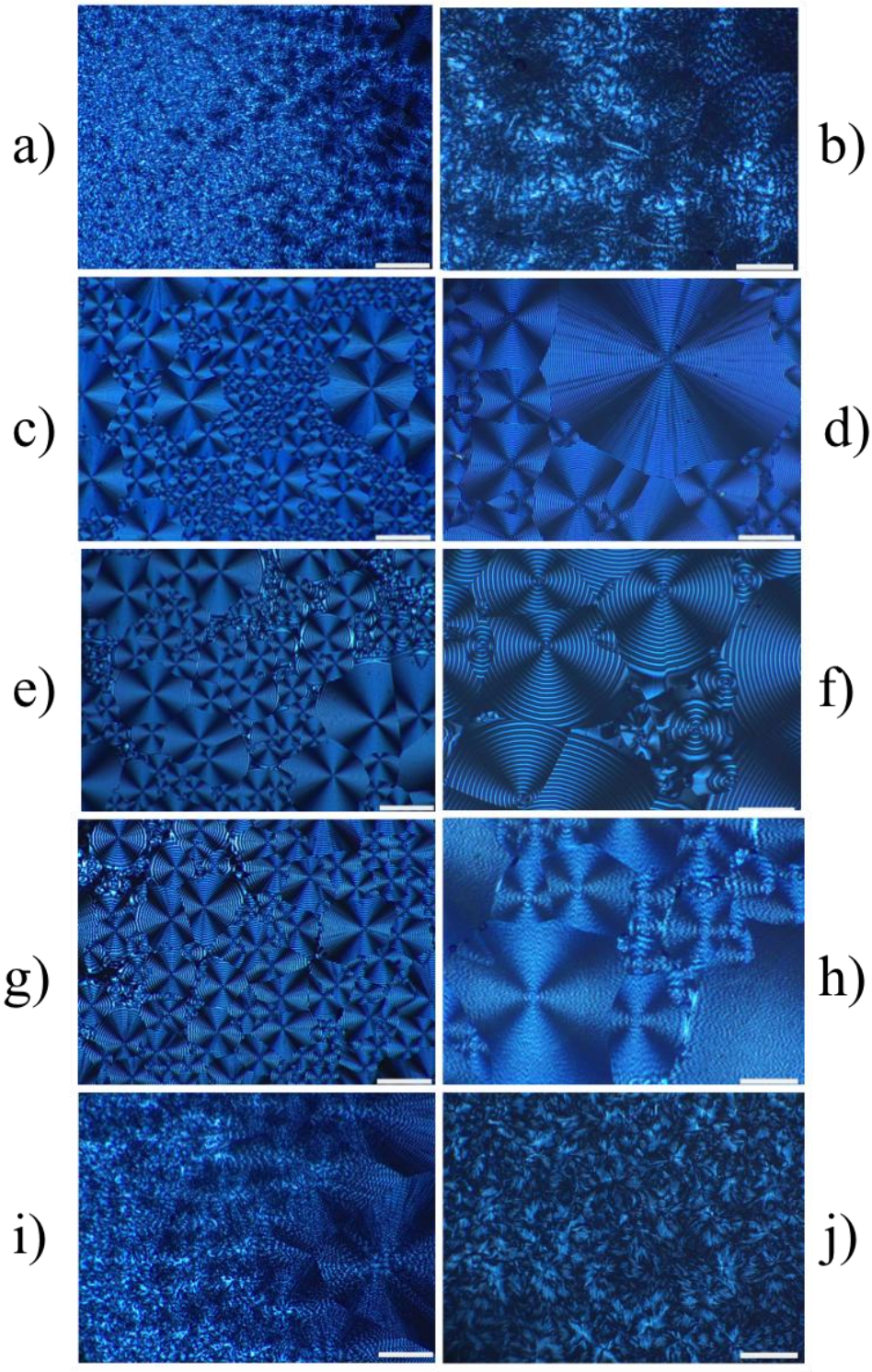

Figure 2. POM micrographs of PHB and blend compositions recorded at 30 °C at two different magnifications (left, 5×, scale bar: 50 μm; right, 20×, scale bar: 20 μm). (a,b) PHB, (c,d) F68-5, (e,f) F68-17, (g,h) F127-5, (i,j) F127-17.

As deducible from Figure 2a,b, PHB crystallized producing a distribution of morphologies including unresolved structures, dendritic and banded spherulites. This heterogeneous morphology agrees with a crystallization process spanning over a wide range of temperatures as determined by DSC and evidenced by the broad, double exothermic crystallization peak reported in Figure 1a. Micrographs recorded on blend composition revealed that the addition of pluronic induced crystal ordering and lamellar twisting leading to the formation of more resolved ringed spherulites. For F68-5 (Figure 2c,d), only double-banded spherulites with constant twist period along the direction of radial growth were visible throughout the overall investigated sample. This sample also showed the highest number density of spherulites with the smallest dimensions (Figure 2c,d). Less ordered domains started appearing by increasing the F68 content to 17% (Figure 2e,f). However, double-banded spherulites with larger average dimension and band periodicity still dominated the F68-17 morphology. In the case of pluronic F127 blends, the structure was less ordered than in the case of F68, in good agreement with the lower values of relative crystallinity found from DSC analysis. In particular, F127-5 blend was mostly composed of different types of banded spherulites with different twist periods together with very small less ordered domains (Figure 2g,h). The increase of F127 content to 17% dramatically changed the final structure leading to a wide distribution of morphologies ranging from very large banded spherulites to less ordered dendritic spherulites and totally unresolved domains (Figure 2i,j).

The observed results may be explained in terms of crystallization kinetics of polymer blends. Binary polymer blends exhibit a wide range of supramolecular structures and morphologies depending on their miscibility and their capability to crystallize under the experimental conditions. Generally speaking, the spherulitic growth rate of a crystallizable polymer in a miscible blend is governed by dilution effects, diffusion of

the constituent macromolecules, and the T_g of the blend [53]. For low interacting polymers (as in the case of PHB and pluronics), the overall crystallization process is mainly determined by kinetic factors that ultimately drive the final structural arrangement [54,55]. Based on the theory developed by Keith and Padden (KP theory) [56], the final blend morphology is qualitatively established by the interplay between the growth rate of the HTC (higher temperature crystallizing) blend component and the diffusive displacement rate of the LTC or NCC (lower temperature crystallizing or not crystallizing) blend component that acts as a diluent. Accordingly, longer segregation scales are expected for more mobile diluents. Thus, the structure is controlled by the so-called diffusion length, δ, defined as the ratio between the diffusivity of the diluent, D, and the crystals' radial growth rate, G [57]. At high undercooling, δ is small and the uncrystallizable polymer cannot escape the envelope of the spherulite. As a consequence, a remarkable amount of the diluent is trapped into the growing semicrystalline structures and the spherulites grow dendritically with an irregular internal order or even open structure [58]. At low undercooling, the diluent possesses higher mobility (larger δ) so a significant amount can be found beyond the spherulite envelope: the increase of diluent concentration into the melt at the growth front of the spherulites reduces the spherulite growth rate thus favoring the formation of compact and well-organized structures.

As mentioned above, F68-5 possessed the most ordered morphology exclusively composed of double-banded spherulites. This sample also showed the highest degree of crystallinity (Table 1). According to the T_c and T_0 values reported in Table 2, for F68-5 crystallization occurred at a lower undercooling than for F68-17 blend composition so allowing the diffusion of pluronic out of the crystal growing front. Thus, PHB spherulites could grow to achieve a strikingly regular and dense internal structure

with a sharp and regular surface. For such highly ordered packing, lamellar twisting occurs to release the compressive stress arising from the opposing lamellar fold surfaces. When F68 amount is increased, it imparted an increased mobility to PHB chains: this causes the rise of crystallization induction time, thus decreasing T_c and T_0. Moreover, at lower crystallization temperatures, the diffusivity of the diluent is lower: at least part of the diluent could be included in the interfibrillar regions of the growing spherulites coarsening their structures and producing a heterogeneous morphology composed of both disordered domains and highly ordered banded spherulites.

Regarding the blends containing pluronic F127, we observed that ringed spherulites with different twist periods filled most of the space for F127-5 blend. As deducible from Table 2, crystallization kinetics for samples F127-5 and F68-5 were analogous with very similar T_0, T_c and Avrami parameters. However, F127 possessed a higher molecular weight than F68 which certainly reduced its diffusion rate and, therefore, its segregation level. The inclusion of even a minute amount of the diluent within the growing spherulite could induce its disordering and produce composition gradients responsible for the formation of spherulites with different periodicity, as those observed in the F127-5 sample.

As for sample F68-17, the distribution of morphology and the presence of less resolved domains observed for the F127-17 blend could be explained by the growth and diffusion rate interplay that, at larger undercooling, does not favor the production of compact, regular, ringed spherulites. The coarsening observed for this sample as compared to the analogous blend containing F68 could be at least partly explained by the lower diffusion rate of F127 and, therefore, its remarkable incorporation within the inner structure of spherulites that consequently grew unevenly with low internal order

and an irregular surface. The hypothesized slightly higher compatibility of F127 with PHB could also be taken into account.

3.4 SAXS-WAXS analysis

The sub-cell packing of PHB and blend compositions was determined by WAXS (Figure 3b). As expected, the curves were the superimposition of those of neat PHB and pure pluronics. All WAXS profiles were dominated by peaks at 2θ = 21.5° and 22.8° corresponding to an orthorhombic packing of the polymer chains within the crystalline layer of the lamellae. This finding agrees with results reported in the literature according to which PHB crystallizes in an orthorhombic cell [59].

The profile for F127-17 blend also showed a peak at 2θ = 19° (labeled with an asterisk in Figure 3b) which indicated the presence of crystalline F127 in the as-prepared blend film already evidenced by DSC.

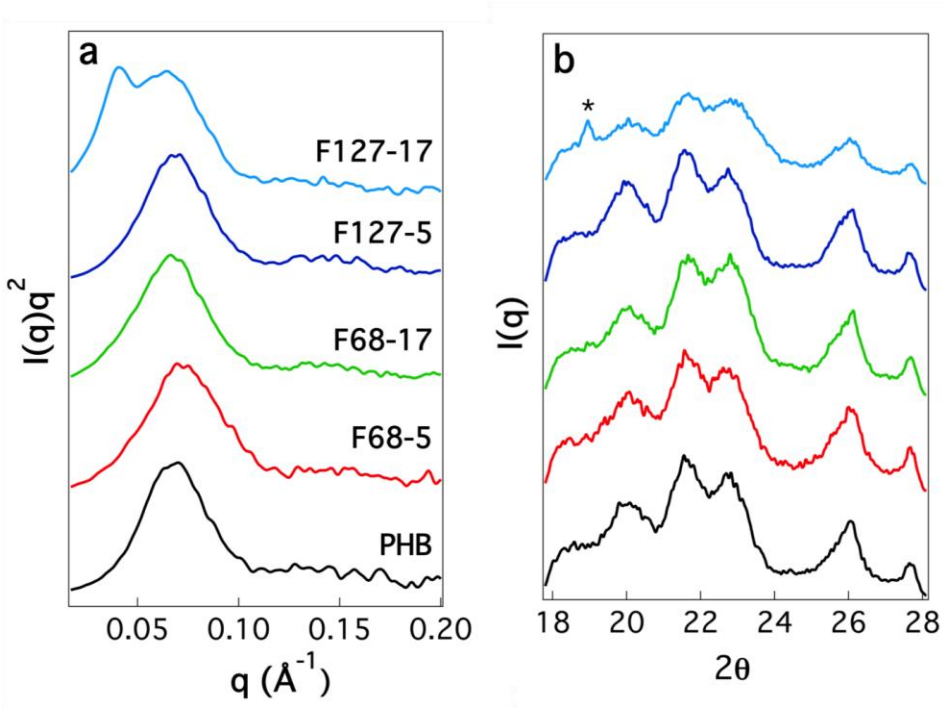

Figure 3. (a) Lorentz-corrected plots and (b) WAXS profiles for neat PHB and PHB/pluronic blend compositions. The curves have been displaced vertically for clarity. The asterisk indicates the diffraction peak due to crystalline F127.

SAXS experiments were performed to characterize the nanostructure of as-prepared PHB and PHB/pluronic blends, mainly to clarify the mutual position of the crystalline and amorphous elements. Indeed, the final properties of homopolymers and blends are distinctively affected by the location of the amorphous component [60]. SAXS profiles of neat PHB and the as-prepared blends are shown in SI, Figure S3, while Figure 3a shows the Lorentz-corrected plots $I(q)$ versus q^2. All samples showed one peak at about q = 0.07 Å^{-1} due to the first order of the crystalline lamellar repeat (or long period LP). The curve for F127-17 showed an extra peak at lower q-value (q = 0.04 Å^{-1}) which could be ascribed to F127 crystals formed during the film preparation by thermomoulding. For all investigated samples LP, computed from the Bragg law, was about 9 nm with a subtle decrease for F68-5 blend composition, meaning that the overall lamellar thickness did not increase upon blending (Table 3).

The morphological parameters associated with the lamellar domains can be also obtained by the 1D-correlation function, γ(z), whose first maximum correponds to the overall lamellar thickness, L. The γ(z) functions were calculated for neat PHB and all blend compositions with the exception of F127-17 due to the co-existence of PHB and F127 crystals; γ(z) obtained for PHB is reported in Figure S4, SI, as an example. The so-obtained L values are listed in Table 3, together with the crystalline and amorphous layer thicknesses (l_c and l_a, respectively) and the linear crystallinity ϕ_c^{lin} defined as l_c/L also obtained by γ(z) function calculation.

Table 3. Structural parameters for neat PHB and PHB/pluronic blends. Long period, LP, obtained from Lorentz-corrected plots, long period, L, thickness of

crystalline and amorphous layers (l_c and l_a, respectively), linear crystallinity, ϕ_c^{lin}, and correlation length, a_c, obtained by Debye-Beuche equation.

Sample	LP (nm)	L (nm)	l_c (nm)	l_a (nm)	ϕ_c^{lin}	a_c (nm)
PHB	9.1	9.0	3.1	5.9	0.34	5.5
F68-5	8.5	7.9	3.3	4.6	0.41	6.7
F68-17	9.4	9.2	3.5	5.7	0.38	6.6
F127-5	9.1	8.8	3.0	5.8	0.34	7.3
F127-17	9.0	9.2	-	-	-	7.1

The crystalline thickness l_c remained approximately constant for all specimens in agreement with the approximately constant melting points recorded by DSC. L was also constant for all samples, except for the F68-5 blend composition that exhibited a subtle decrease of L from 9 nm to 8 nm accompanied by an analogous decrease of the amorphous layer thickness, l_a. The PHB lamellar morphological parameters did not change upon blending meaning that pluronics underwent extralamellar segregation during PHB crystallization forming pluronic-rich amorphous domains outside the lamellar region. The complete incorporation of pluronic in the lamellar stacks would have resulted into a monotonic increase of both LP and l_a, which was not observed. The extralamellar placement of amorphous diluents has been already reported in the literature for binary polymer blends. Two driving forces are invoked to explain the phenomenon: the entropic gain associated with the tendency of the diluent to resume random-coiled conformation and the crystallization of crystallizable segments in the interlamellar regions. These two forces compete against the favorable interaction between the diluent and the amorphous portion of the crystalline polymer in the interlamellar regions [61]. The segregation degree of pluronic outside the lamellar

domains appeared to be slightly more pronounced for F68 than for F127 as indicated by the amorphous layer thickness decrease (≈ 1 nm) observed for F68-5. The slightly different behavior observed for the two investigated pluronics might be explained by the higher hydrophilic character of pluronic F68 (HLB = 29) with respect to F127 (HLB = 22) that could slightly lower its compatibility with the highly hydrophobic PHB. Moreover, analogously to what previously reported for PVC/PCL blends [61], the higher molecular weight of F127 reduced its diffusion coefficient making it unable to efficiently escape the spherulite envelope during PHB crystallization.

The remarkable segregation of F68 outside PHB lamellae might favor the interactions between the PHB crystallizable segments increasing the final specimen crystallinity thus explaining the higher linear crystallinity, ϕ_c^{lin}, values determined for PHB/F68 blend compositions. The ϕ_c^{lin} values extrapolated from γ(z) functions agreed with the crystallinity degree values obtained by DSC. The small discrepancies observed for F68-17 and F127-5 blend compositions might reside in the fact that SAXS only probes the crystallinity inside lamellar stacks, while DSC accounts for the overall sample crystallinity. Poorly crystallized domains with ill-defined lamellar structure or disordered regions at spherulitic boundaries contribute to the observed SAXS-DSC differences. Accordingly, the most significant discrepancies between the crystallinity values obtained with the two techniques were recorded for samples featured by polydisperse morphology, i.e. F68-17 and F127-5. The ϕ_c^{lin} and ϕ_c values also paralleled for neat PHB indicating that also for the homopolymer crystallinity mostly resided within the lamellar domains.

The formation of amorphous extralamellar inhomogeneities was confirmed by the rise of the scattering intensity observed in the in the low-q region of the SAXS profiles for all specimens (see Figure S3 in SI). As suggested by Nojima and co-workers [62,63],

SAXS curves could be described as the superposition of intensities arising from a two-phase structure system consisting of crystalline regions and inhomogeneities associated to amorphous extralamellar domains. Assuming that the lamellar domains and the extralamellar amorphous inhomogeneities were randomly distributed and that the contribution to the scattering intensity at low q due to the alternating lamellar layers was negligible, the low-q intensity could be described by the Debye-Beuche equation that allowed calculating the correlation length, a_c, associated to the size of the amorphous extralamellar domains:

$$I(q) = \frac{A}{(1 + {a_c}^2 q^2)^2} \qquad (9)$$

where A is a constant and a_c is the correlation length.

The straight line yielded by the plot $\mathrm{I(q)}^{-\frac{1}{2}}$ versus q^2 has slope of $a_c^2 \cdot A^{-\frac{1}{2}}$ and intercept of $1 \Big/ A^{-\frac{1}{2}}$. The correlation length can thus be obtained from the ratio between the slope and the intercept. The so-obtained a_c values are reported in Table 3. Interestingly, also neat PHB possessed amorphous extralamellar domains meaning that not all amorphous component could be entirely accommodated inside the lamellae during the crystallization of the homopolymer. The size of the amorphous extralamellar inhomogeneities increased from 5.5 nm to about 7 nm upon blending confirming the segregation of pluronics in extralamellar regions occurred during blend preparation. For all blends, the a_c values were larger than both l_c and l_a suggesting that blends had developed heterogeneities with larger size than the two types of layers.

The development of amorphous extralamellar domains for neat PHB was confirmed by calculating the volume fraction of lamellar stacks in the sample, ϕ_s, that, for volume

filling spherulites, can be obtained by comparing the linear crystallinity, ϕ_c^{lin}, to the bulk crystallinity, ϕ_c [40]:

$$\Phi_c = \Phi_s \cdot \Phi_c^{lin} \qquad (10)$$

ϕ_c is calculated by means of the crystallinity degree obtained by DSC, X_c, as follows [64]:

$$\Phi_c = X_c \left(\frac{\rho_s}{\rho_c}\right) \qquad (11)$$

where ρ_s corresponds to the overall density of the sample and ρ_c is the density of the crystalline fraction.

The overall density ρ_s can be calculated by the following equation:

$$\rho_s = X_c\rho_c + (1 - X_c)\rho_a \qquad (12)$$

where ρ_a is the density of the amorphous phase. The calculation could be performed only for pure PHB since values for ρ_c and ρ_a are not available for both F68 and F127. The values used for ρ_c and ρ_a for neat PHB are 1.260 and 1.177 g cm^{-3}, respectively [65].

The X_c value for neat PHB obtained from the first heating ramp was 0.29. The calculated values of ϕ_c and ϕ_c^{lin} were 0.28 and 0.34, respectively, which led to a value of ϕ_s of about 0.8, lower than unity. ϕ_s provides a measure of the extent of interlamellar incorporation of amorphous PHB. When all amorphous polymer is incorporated in the interlamellar region, the whole volume is filled with lamellar stacks and ϕ_s is equal to 1; when part of the amorphous component is placed outside the lamellar domains, ϕ_s is below 1. In the present work, ϕ_s = 0.8, meaning that amorphous PHB was partially expelled from the interlamellar region. Based on the assumption of volume filling spherulites, we could argue that amorphous PHB was partially segregated in the

interfibrillar space. Nevertheless, its extra-spherulites placement could not be totally excluded.

In summary, we can conclude that, except for the blend F127-17 that is close to the unstable region of the phase diagram, PHB and pluronics were miscible in the melt in the investigated range compositions, pluronics were prevented from crystallization and PHB crystallized producing a rather complex system where the amorphous material could not be fully accommodated in homogeneous amorphous interlamellar layers but was partly segregated in amorphous extralamellar regions. Liquid-liquid demixing between PHB and pluronics, that has often been invoked to explain the crystallization behavior of several binary polymer blends that show the formation of extralamellar amorphous inhomogeneities [66,67], could be responsible for the observed behavior. Indeed, due to the dissimilarity of chemical structure and to entropic factor related to geometrical asymmetry [68], PHB and pluronics, miscible close to the melting point, started demixing at a certain temperature above the crystallization temperature and at least part of the pluronics was rejected out from the interlamellar region to form pluronic-rich domain outside PHB lamellar stacks.

3.5 Non-isothermal crystallization behavior by rheometry

Beyond calorimetric analysis, rotational rheometry under the same cooling conditions used for DSC experiments was applied to investigate the non-isothermal crystallization kinetics of neat PHB and PHB/pluronic blends. The main advantages of rheometry are: (1) it is much easier and faster than other methods such as optical microscopy, small-angle light and X-ray scattering and differential scanning calorimetry, (2) even small polymer microstructure modifications can be detected by measuring the mechanical spectrum, and (3) it can be applied to systems that cannot be investigated by other methods, such as colored and filled composite systems [69].

However, despite being rheometry a complementary tool to study the crystallization kinetics due to its higher sensitivity as compared to conventional methods, the interrelation between the relative crystallinity and the mechanical data is not simple and remains a topic open to discussion [70,71].

Figure 4 shows the evolution of storage modulus, G', with time, measured during the non-isothermal crystallization (Figure 4a) and its logarithmic normalization, $G_n(t)$, (Figure 4b) for neat PHB and PHB/pluronic blend compositions. Table 4 lists the values of the storage modulus at the beginning of the crystallization process, G'_{min}, the value obtained by the last measurable plateau, G'_{max}, the crystallization onset temperature, $T_{0\,rheo}$, and the crystallization half-time, $t_{1/2}$rheo, as determined by dynamic mechanical tests.

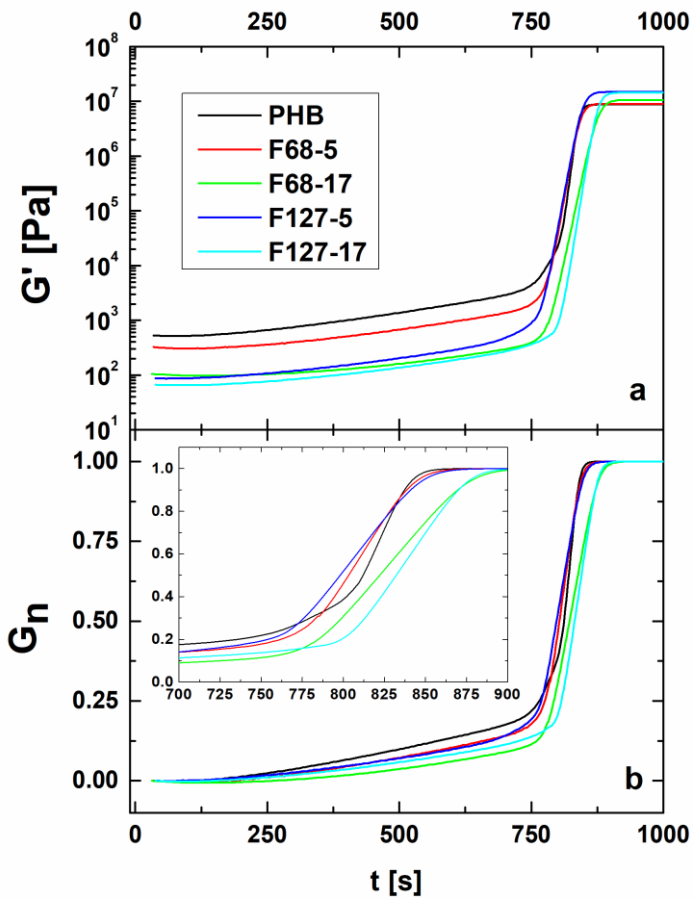

Figure 4. a) Time evolution of storage modulus, G' and b) Time evolution of normalized storage modulus (i.e relative crystallinity), $G_n(t)$, for neat PHB and PHB/pluronic blend compositions.

The evolution of G' as a function of time showed the typical sigmoidal shape according to which G' progressed from about constant values at the beginning of the process to an abrupt increase at the onset of crystallization, and finally reached a plateau. During crystallization, G' rises due to filler effects of crystals growing in an amorphous matrix [69]. The slight initial G' increase recorded during the induction time (i.e. the time at the intersection of the highest slope of the storage modulus-time curve with the line through the initial almost constant storage modulus values) could be attributed to a premature crystallization during cooling [72]. Furthermore, the initial value of G', G'_{min}, decreased upon blending, with F127-17 blend composition possessing the lowest G'_{min}.

In order to compare results obtained by calorimetry and rheometry, the change of the relative crystallinity versus time must be derived from rheology experiments. According to Pogodina and co-workers [70], for dynamic mechanical tests, the relative crystallinity can be estimated by applying a logarithmic normalization of G'.

The so obtained normalized storage modulus $G_n(t)$ can be expressed as follows:

$$G_n(t) = \frac{\log G'(t) - \log G'_{min}}{\log G'_{max} - \log G'_{min}} \qquad (9)$$

where G'_{min} and G'_{max} are the values of G' at the beginning and at the ending plateau of storage modulus, respectively.

Table 4. Storage moduli at the beginning of the crystallization process, G'_{min}, at the ending plateau, G'_{max}, onset temperature, $T_{0\,rheo}$, and half-time, $t_{1/2\,\mathrm{rheo}}$, determined by rheology.

Sample	G'_{min} (Pa)	$G'_{max} \times 10^6$ (Pa)	$T_{0\,rheo}$ (ºC)	$t_{1/2\,\mathrm{rheo}}$ (min)
PHB	526.3	8.8	117.3-113.9	13.56
F68-5	321.9	9.1	115.9	13.38
F68-17	104.8	10.7	114.6	13.69
F127-5	86.8	15.1	115.9	13.30
F127-17	66.8	14.5	111.2	13.88

All curves showed an induction period where premature crystallization was assumed to occur. It is worth noting that the applied stress was small enough to avoid any disturbance in the crystallization kinetics and was adjusted previously to obtain a low torque level compatible with the transducer sensitivity. Nevertheless, the sigmoidal curves were shifted towards shorter times for rheological measurements as compared to DSC experiments, possibly suggesting a shear-induced crystallization behavior. Moreover, relative crystallinity values determined for PHB and F127-17 sample just after the induction time were 20% and 15%, respectively, both larger than the analogous virtually nil X_t values determined by DSC. Besides, the relative crystallinity versus time curves obtained by rheology (Figure 4b) and by DSC (Figure 1b) were not quantitatively superimposable suggesting that rheology might represent a more sensitive tool than differential scanning calorimetry to follow a polymer crystallization process, particularly at its very early stage. Indeed, while the crystallinity development during the induction period cannot be detected by DSC, the premature crystals' appearance was clearly evidenced by the slow increase of polymer viscoelasticity.

Despite the just mentioned discrepancy at the beginning of crystallization, rheology and DSC provided several consistent results. First, the onset temperature (taken as the temperature at which $G_n(t)$ starts to rapidly increase), $T_{0\,rheo}$ (Table 4) decreased upon blending and, within each PHB/pluronic system, by increasing the pluronic content. Thus, the delaying effect played by pluronics on PHB crystallization deduced by DSC was further proved. As already mentioned, the values for both crystallization and onset temperatures determined by rheology were significantly smaller than those obtained by DSC, indicating that PHB crystallization could be promoted by the flow field imposed in rheological experiments. Further experiments should be performed in order to verify this hypothesis.

Second, the curve of the relative crystallinity versus time for neat PHB (Figure 4b) showed two different regions with different slopes that could be ascribed to the formation of two kinds of crystallites during the crystallization process. In particular, a first slower crystallization was followed by a faster crystal growth phase indicating that PHB crystallization is a complex process spanning over a wide range of temperature. This slope variation paralleled the double crystallization peak showed by PHB in DSC experiments reported in Figure 1a. Thus, both DSC and rheological tests indicated that crystallinity evolved in two different ways for neat PHB and PHB/pluronic blends: while crystallinity mostly developed through a two-step process for the former, crystallization proceeded via a one-step mechanism for the latter.

The quantitative effect of both the amount and nature of pluronics on the non-isothermal crystallization kinetics of PHB/pluronic blends was derived from $G_n(t)$ versus time sigmoids by determining the crystallization half-time, $t_{1/2\text{rheo}}$, defined as the time at which the relative crystallinity reached a value of 0.5. It is worthwhile to note that $t_{1/2\text{rheo}}$ values were not obtained by Avrami analysis since the

shape of the rheological curves could not be accounted by the Avrami equation providing unreasonably high exponents ($n \approx 8$). The values of $t_{1/2}^{\text{rheo}}$ reported in Table 4 showed that, within each PHB/pluronic blend series, the time required to complete 50% of the crystallization process increased by increasing the pluronic content, in agreement with the absolute half-time values extracted by the X_t versus time curves reported in Figure 1b (see values of $t_{1/2}^{\text{DSC}}$ reported in Table S1 in SI). Indeed, the viscoelastic response of a material is directly correlated with its structure and its evolution during the crystallization process which does not only depend on the crystal volume fraction variation, but also on the viscoelastic properties and interactions between the different ordered and disordered developing phases (i.e. the disordered melt phase that is transforming to solid and the solid phase which combines ordered domains with disordered solid material unable to crystallize) [73]. In contrast, $t_{1/2}^{\text{rheo}}$ for F68-5 and F127-5 specimens were smaller than that obtained for neat PHB, not following the trend obtained by DSC measurements. This lack of congruence might be related to the different sensitivity of the two employed techniques.

Contrary to what was expected, F127-containing blends, which showed lower X_c values (Table 1) than analogous blends containing F68, possessed the largest G'_{max}. Nevertheless, in agreement with the higher crystallinity degree obtained by DSC, all blends showed more pronounced elastic behavior than neat PHB. The observed rheology/DSC inconsistency might be rationalized by considering the strength of spherulite-spherulite interaction. G'_{max} value is known to decrease by lowering the strength of interspherulite interactions [74]. As previously discussed, F68-5 possessed the most pronounced segregation degree of pluronic outside the lamellar domains. Therefore, despite the large overall crystallinity degree, X_c, the presence of pluronic between adjacent spherulites could weak their connectivity lowering the final G'_{max}

value. On the other hand, the lower liquid-liquid demixing extent revealed for F127-containing blends could enhance the interaction between adjacent spherulites, thus enhancing the elastic behavior.

To further investigate the effect of pluronics on PHB crystallization, the change of complex viscosity, η^*, with temperature was recorded for neat PHB and all blends (Figure 5). Moreover, η^* trends further supported miscibility between PHB and pluronic in the molten state hypothesized based on DSC results. η^* decreased upon blending and by increasing pluronic content meaning that blending resulted into lowered interaction densities.

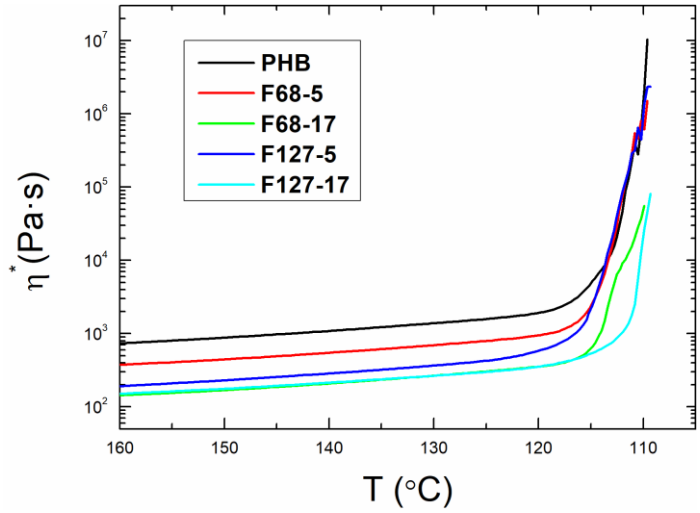

Figure 5. Change of complex viscosity, η^*, with temperature for neat PHB and PHB/pluronic blends.

Interestingly, despite the higher F127 molecular weight, η^* drop was found to be larger for F127-5 than for F68-5. As already mentioned, we might argue that the slightly higher hydrophilic character of pluronic F68 than F127 could lower PHB-pluronic interactions enhancing the pluronic segregation also in the molten state and thus increasing the viscosity.

3.6 Tensile properties

Table 5 reports the mechanical properties (ultimate tensile strength, σ_f, strength at break, σ_b, elongation at break, ε_b, and Young's modulus, *E*) for all as-prepared specimens. In the case of F127-17 blend, mechanical tests were not performed due to its inhomogeneous morphology responsible for particularly fragile samples.

The mechanical properties of polymer blends depend on several factors such as the properties of the individual constituents, their degree of compatibility, the mode of dispersion, etc. In crystallizable polyblends the mechanical behavior is also affected by the degree of crystallinity, the ability to co-crystallize, the morphology, and the compatibility in the amorphous state [75]. Moreover, polymer blends usually possess a more complex structure than homopolymers due to the occurrence of a dispersed phase, a continuous phase, and the polymer-polymer interface featured by a finite thickness. Being the applied force transmitted onto the dispersed phase from the matrix via the interface, the latter plays a vital role on the overall blend behavior [76].

Table 5. Ultimate tensile strength, σ_f, strength at break, σ_b, elongation at break, ε_b, and Young's modulus, *E*, for neat PHB and PHB/pluronic blends.

Sample	σ_f (MPa)	σ_b (MPa)	ε_b (%)	E (MPa)
PHB	20.95 ± 4.72	17.79 ± 4.76	20.29 ± 11.06	430.52 ± 73.09
F68-5	17.63 ± 2.90	16.27 ± 3.40	11.35 ± 2.17	443.15 ± 37.34
F68-17	15.91 ± 4.16	15.61 ± 4.02	7.71 ± 3.19	517.15 ± 119.85
F127-5	17.53 ± 3.34	16.83 ± 3.09	6.99 ± 2.04	649.37 ± 175.10

The values listed in Table 5 indicate that blending resulted into a decrease of the elongation at break and an increase of Young´s modulus: for F68-containing blends, E increased with increasing the pluronic content from about 430 MPa for neat PHB to 443 MPa and 517 MPa for F68-5 and F68-17, respectively. The increase was even larger upon addition of F127 reaching a value of 649 MPa for F127-5. These findings clearly indicate an enhanced brittle behavior of blends as compared to neat PHB.

Typically, more crystalline materials possess higher Young's modulus; nevertheless, this linear trend was not found in the present study. Indeed, F68-5 possessed the smallest Young's modulus (443 MPa) and the largest crystallinity degree X_c (42.6%), while F127-5 showed the highest Young's modulus (649 MPa) and a smaller value of X_c (37.1%). Clearly, the elastic behavior of the investigated PHB/pluronic blend compositions could not be simply explained in terms of their degree of crystallinity or lamellar thickness. As a matter of fact, the blend nano- and micro-structure must be taken into account. Amorphous domains possess different energy dissipation power depending on their exact location with respect to spherulites [64]. Thus, highly segregated F68-rich amorphous domains present at the interspherulitic boundaries in F68-5 specimen might possess a higher capability to dissipate energy which gave rise to the unpredictable mechanical properties recorded for this highly crystalline sample. On the other hand, the partial inclusion of F127 in the inner structure of spherulite assumed for F127-5 sample based on POM and SAXS experiments could enhance the interphase elastic contribution leading to the recorded increase of Young's modulus.

Another observation is that blending reduced the sample elongation capability: the elongation at break, ε_b, decreased from 20.29% for neat PHB to 11.35% for F68-5 and further to 7.71% and 6.99% for F68-17 and F127-5, respectively. It is well known that spherulite size pronouncedly affects the deformation of semicrystalline polymers with

polymer brittleness increasing by increasing spherulite radius [77–79]. Moreover, more heterogeneous structures certainly show inter-domain higher degree of voids and imperfections that are known to provide relatively easy paths for crack propagation at the interface, thus reducing the sample elongation capability. POM investigation revealed that F68-5 morphology was highly homogeneous and composed of many small spherulites, while the other blends possessed a coarse structure composed of larger well- and ill-defined spherulites and less ordered domains. This, combined with the larger spherulitic size observed for F68-17 and F127-5, could well explain the lower values of ε_b determined for these blends as compared to the more crystalline F68-5 sample. This behavior was further emphasized for F127-17 blend, whose remarkably inhomogeneous morphology containing banded, dendritic and unresolved spherulites resulted into extremely low ε_b values (few percent) and a catastrophic failure during tensile tests. The general lower elongation resistance of blends with respect to neat PHB was further enhanced by the significantly lower molecular weight of pluronic.

The addition of pluronics to PHB reduced its ability to resist breaking under tensile stress: both the ultimate strength, σ_f, and the strength at break, σ_b, decreased upon blending. The reduction increased by increasing the pluronic content. Again, the morphology revealed by POM and SAXS investigation can be invoked to explain these findings. In order to resist to applied loads, the amorphous regions between adjacent crystals must be capable to accommodate some crystals' rotation [80]. We can hypothesize that in our samples the amorphous regions were too constrained to adjust accordingly and, upon distortion, the amorphous chains tightened up immediately, producing a brittle fracture. Shen et al. have recently demonstrated that the interface between crystals of two different components in a polymer blend is weaker than that between identical crystals arising from a less perfect lattice matching [74]. Thus, PHB-

pluronic interface might be weaker than the PHB-PHB one and, therefore, less efficient towards stress transfer, thus explaining the blend scarce resistance towards tensile stresses.

4. Conclusions

Addition of pluronic F68 or F127 to PHB produced macroscopically homogeneous blend films by simple thermomoulding. Four binary blend compositions were prepared containing 5 and 17 wt% of pluronics. For all blends, the two components were found to be miscible in the amorphous state. Moreover, blending delayed the crystallization process though increasing the overall final crystallinity degree. The mechanism of crystal growth changed depending on the pluronic content: 3-dimensional solids sheaf growth was observed for blend compositions containing 5 wt% of both pluronic, while 3D spherical growth with athermal nucleation featured both blends containing 17 wt% of pluronics and neat PHB.

The different crystallization mechanisms led to significant variations of the final sample morphology and nanostructure as revealed by polarized optical microscopy (POM) and small- and wide-angle X-ray scattering (SAXS, WAXS). In particular, addition of pluronics promoted crystal ordering with the formation of more resolved ringed spherulites with respect to neat PHB which showed a polydisperse inhomegenous structure. Besides, for such low interacting polymer systems, the final morphology was found to be mainly controlled by the diffusion rate of pluronics: the higher the diffusion coefficient, the higher the spherulite crystalline ordering. Thus, the more diffusive F68 led to highly homogeneous samples mostly composed of double-banded spherulites with constant twist period. Crystal ordering paralleled the segregation extent of pluronic in extralamellar amorphous domain. Indeed, the smaller

size and the lower chemical compatibility of F68 towards PHB enhanced its capability to escape the spherulite envelope with subsequent formation of compact and well-organized spherulitic structures. This effect was particularly evident for F68-5 blend composition where only small double banded spherulites with constant twist period filled the overall sample volume.

All blend compositions showed higher Young's modulus and lower elongation at break than neat PHB, in agreement with the increased crystallinity observed upon blending. Unexpectedly, among blends, the most crystalline F68-5 sample was also the less brittle. We argued that the highly segregated F68-rich amorphous domains present at the interspherulitic boundaries of this specimen could better dissipate energy thus explaining the recorded mechanical properties. On the other hand, the more heterogeneous structure observed for F127-based blends could account for the poor mechanical behavior recorded for F127-5 and, especially, F127-17 blends.

The present study shows that the non-isothermal crystallization behavior of PHB and PHB/pluronic blends can be studied both by differenial scanning calorimetry and rheometry. The two techniques provided analogous results in terms of crystallinity evolution, but rheometry appeared to be extremely powerful to follow the early stage of crystallization which is inaccessible by DSC. Moreover, rheology allowed monitoring the crystallization process in a rather straightforward way that does not necessitate considerable data analysis. Thus, rheology represents a valuable tool whose full potential to investigate polymer blends' crystallization behavior has not yet been exploited.

Acknowledgments

The authors would like to acknowledge the Ministero dell'Istruzione, dell'Università e della Ricerca (MIUR, Rome), the Erasmus+ Programme, the Consorzio Interuniversitario per lo Sviluppo dei Sistemi a Grande Interfase (CSGI), and the Chemical Process and Product Technology Research Center (Pro2TecS) of the University of Huelva (Huelva, Spain) for financial support.

Research data for this article

Data not available/Data will be made available on request.

Appendix A. Supplementary material

Glass transition temperatures' deviations from linearity, DSC thermogram of F127-17 blend, SAXS curves for all blend films and an example of 1D correlation function obtained from SAXS analysis, crystallization half-times of all samples obtained from both DSC and rheology measurements.

References

[1] S. Ebnesajjad, Handbook of biopolymers and biodegradable plastics: properties, processing and applications, William Andrew, 2012.

[2] R. Jayakumar, D. Menon, K. Manzoor, S.V. Nair, H. Tamura, Biomedical applications of chitin and chitosan based nanomaterials—A short review, Carbohydr. Polym. 82 (2010) 227–232.

[3] G. Koronis, A. Silva, M. Fontul, Green composites: a review of adequate materials for automotive applications, Compos. Part B Eng. 44 (2013) 120–127.

[4] S. Van Vlierberghe, P. Dubruel, E. Schacht, Biopolymer-based hydrogels as scaffolds for tissue engineering applications: a review, Biomacromolecules. 12 (2011) 1387–1408.

[5] M. Lemoigne, Products of dehydration and of polymerization of β-hydroxybutyric acid, Bull Soc Chem Biol. 8 (1926) 770–782.

[6] R.A.J. Verlinden, D.J. Hill, M.A. Kenward, C.D. Williams, I. Radecka, Bacterial synthesis of biodegradable polyhydroxyalkanoates, J. Appl. Microbiol. 102 (2007) 1437–1449. doi:10.1111/j.1365-2672.2007.03335.x.

[7] P.L. Gould, S.J. Holland, B.J. Tighe, Polymers for biodegradable medical devices. IV. Hydroxybutyrate-valerate copolymers as non-disintegrating matrices for controlled-release oral dosage forms, Int. J. Pharm. 38 (1987) 231–237. doi:10.1016/0378-5173(87)90119-0.

[8] J. Chen, S.S. Davis, The release of diazepam from poly(hydroxybutyrate-hydroxyvalerate) microspheres, J. Microencapsul. 19 (2002) 191–201. doi:10.1080/02652040110065431.

[9] N.K. Singh, B.P. Das Purkayastha, J.K. Roy, R.M. Banik, P. Gonugunta, M. Misra, P. Maiti, Tuned biodegradation using poly(hydroxybutyrate-co-valerate) nanobiohybrids: Emerging biomaterials for tissue engineering and drug delivery, J. Mater. Chem. 21 (2011) 15919. doi:10.1039/c1jm12427g.

[10] C. Ye, P. Hu, M.-X. Ma, Y. Xiang, R.-G. Liu, X.-W. Shang, PHB/PHBHHx scaffolds and human adipose-derived stem cells for cartilage tissue engineering, Biomaterials. 30 (2009) 4401–4406. doi:10.1016/j.biomaterials.2009.05.001.

[11] G.-Q. Chen, Q. Wu, The application of polyhydroxyalkanoates as tissue engineering materials, Biomaterials. 26 (2005) 6565–6578. doi:10.1016/j.biomaterials.2005.04.036.

[12] C.W. Pouton, S. Akhtar, Biosynthetic polyhydroxyalkanoates and their potential in drug delivery, Adv. Drug Deliv. Rev. 18 (1996) 133–162. doi:10.1016/0169-409X(95)00092-L.

[13] M. Avella, E. Martuscelli, Poly-d-(−)(3-hydroxybutyrate)/poly(ethylene oxide) blends: phase diagram, thermal and crystallization behaviour, Polymer. 29 (1988) 1731–1737. doi:10.1016/0032-3861(88)90384-9.

[14] M. Avella, E. Martuscelli, P. Greco, Crystallization behaviour of poly(ethylene oxide) from poly(3-hydroxybutyrate)/poly(ethylene oxide) blends: phase structuring, morphology and thermal behaviour, Polymer. 32 (1991) 1647–1653. doi:10.1016/0032-3861(91)90401-4.

[15] A. Bhattacharjee, K. Kumar, A. Arora, D.S. Katti, Fabrication and characterization of Pluronic modified poly(hydroxybutyrate) fibers for potential wound dressing applications, Mater. Sci. Eng. C. 63 (2016) 266–273. doi:10.1016/j.msec.2016.02.074.

[16] P.B. Kajjari, L.S. Manjeshwar, T.M. Aminabhavi, Novel blend microspheres of poly(3-hydroxybutyrate) and Pluronic F68/127 for controlled release of 6-mercaptopurine, J. Appl. Polym. Sci. 131 (2014). doi:10.1002/app.40196.

[17] S. Akhtar, C.W. Pouton, L.J. Notarianni, The influence of crystalline morphology and copolymer composition on drug release from solution cast and melt-processed P(HB-HV) copolymer matrices, J. Controlled Release. 17 (1991) 225–233. doi:10.1016/0168-3659(91)90141-Y.

[18] Y. He, N. Asakawa, Y. Inoue, Biodegradable blends of high molecular weight poly(ethylene oxide) with poly(3-hydroxypropionic acid) and poly(3-hydroxybutyric acid): a miscibility study by DSC, DMTA and NMR spectroscopy,

Polym. Int. 49 (n.d.) 609–617. doi:10.1002/1097-0126(200006)49:6<609::AID-PI426>3.0.CO;2-6.

[19] N. Jiang, H. Abe, Miscibility and morphology study on crystalline/crystalline partially miscible polymer blends of 6-arm Poly(l -lactide) and Poly(3-hydroxybutyrate- co -3-hydroxyvalerate), Polymer. 60 (2015) 260–266. doi:10.1016/j.polymer.2015.01.060.

[20] Z. Qiu, Crystallization Behavior of Miscible Semicrystalline Polymer Blends, in: Cryst. Multiph. Polym. Syst., Elsevier, 2018: pp. 213–237. doi:10.1016/B978-0-12-809453-2.00008-6.

[21] S. Agarwal, C. Speyerer, Degradable blends of semi-crystalline and amorphous branched poly(caprolactone): Effect of microstructure on blend properties, Polymer. 51 (2010) 1024–1032. doi:10.1016/j.polymer.2010.01.020.

[22] K. Hamad, M. Kaseem, M. Ayyoob, J. Joo, F. Deri, Polylactic acid blends: The future of green, light and tough, Prog. Polym. Sci. 85 (2018) 83–127. doi:10.1016/j.progpolymsci.2018.07.001.

[23] M. Avella, E. Martuscelli, M. Raimo, The fractionated crystallization phenomenon in poly(3-hydroxybutyrate)/poly(ethylene oxide) blends, Polymer. 34 (1993) 3234–3240. doi:10.1016/0032-3861(93)90396-R.

[24] L. Zhao, W. Kai, Y. He, B. Zhu, Y. Inoue, Effect of aging on fractional crystallization of poly(ethylene oxide) component in poly(ethylene oxide)/poly(3-hydroxybutyrate) blends, J. Polym. Sci. Part B Polym. Phys. 43 (n.d.) 2665–2676. doi:10.1002/polb.20552.

[25] Y.G. Jeong, T. Hashida, G. Wu, S.L. Hsu, C.W. Paul, Analysis of the Multistep Solidification Process in Polymer Blends, Macromolecules. 39 (2006) 274–280. doi:10.1021/ma051862t.

[26] Zinan Zhang, Fengyuan Yu, Hongbin Zhang, Isothermal and Non-Isothermal Crystallization Studies of Long Chain Branched Polypropylene Containing Poly(ethylene-co-octene) under Quiescent and Shear Conditions, Polymers. 9 (2017) 236. doi:10.3390/polym9060236.

[27] X. Hu, Y. Lu, M. Li, J. Yu, S. Lu, Effect of Montmorillonite on the Crystallization, Rheological and Physical Behavior of Polyamide-6/Polylactic Acid Blends, Polym. Sci. Ser. A. 60 (2018) 229–238. doi:10.1134/S0965545X18020062.

[28] G. Floudas, C. Tsitsilianis, Crystallization Kinetics of Poly(ethylene oxide) in Poly(ethylene oxide)−Polystyrene−Poly(ethylene oxide) Triblock Copolymers, Macromolecules. 30 (1997) 4381–4390. doi:10.1021/ma9616118.

[29] R.J.A. Steenbakkers, G.W.M. Peters, Suspension-based rheological modeling of crystallizing polymer melts, Rheol. Acta. 47 (2008) 643–665. doi:10.1007/s00397-008-0273-4.

[30] Z. Qiu, S. Fujinami, Ã. Motonori KOMURA, Ã. Ken NAKAJIMA, Ã. Takayuki IKEHARA, T. Nishi Ãã, Nonisothermal Crystallization Kinetics of Poly(butylene succinate) and Poly(ethylene succinate), (n.d.). doi:10.1295/polymj.36.642.

[31] Q. Chen, G. Zhang, K. Wang, C. Wang, G. Ding, J. Liu, Crystallization morphology transition of poly(3-hydroxybutyrate) films depending on nucleation temperature under temperature gradient, Macromol. Res. 25 (2017) 303–310. doi:10.1007/s13233-017-5042-8.

[32] M. Avrami, Kinetics of Phase Change. I General Theory, J. Chem. Phys. 7 (1939) 1103–1112. doi:10.1063/1.1750380.

[33] M. Avrami, Kinetics of phase change. II transformation-time relations for random distribution of nuclei, J. Chem. Phys. 8 (1940) 212–224.

[34] M. Avrami, Kinetics of phase change. III: Granulation, phase change and microstructure, J. Chem. Phys. 9 (1941) 177–184.

[35] A. Jeziorny, Parameters characterizing the kinetics of the non-isothermal crystallization of poly(ethylene terephthalate) determined by d.s.c., Polymer. 19 (1978) 1142–1144. doi:10.1016/0032-3861(78)90060-5.

[36] J.-B. Zeng, Q.-Y. Zhu, Y.-D. Li, Z.-C. Qiu, Y.-Z. Wang, Unique Crystalline/Crystalline Polymer Blends of Poly(ethylene succinate) and Poly(*p* -dioxanone): Miscibility and Crystallization Behaviors, J. Phys. Chem. B. 114 (2010) 14827–14833. doi:10.1021/jp104709z.

[37] T.N. Blanton, M. Rajeswaran, P.W. Stephens, D.R. Whitcomb, S.T. Misture, J.A. Kaduk, Crystal structure determination of the silver carboxylate dimer [Ag(O2C22H43)]2, silver behenate, using powder X-ray diffraction methods, Powder Diffr. 26 (2011) 313–320. doi:10.1154/1.3661981.

[38] W. Ruland, Small-angle scattering of two-phase systems: determination and significance of systematic deviations from Porod's law, J. Appl. Crystallogr. 4 (1971) 70–73. doi:10.1107/S0021889871006265.

[39] G.R. Strobl, M. Schneider, Direct evaluation of the electron density correlation function of partially crystalline polymers, J. Polym. Sci. Polym. Phys. Ed. 18 (1980) 1343–1359. doi:10.1002/pol.1980.180180614.

[40] M.S. Park, J.K. Kim, Phase behavior and crystallization of a poly (ethylene oxide)/cellulose acetate butyrate blend, J. Polym. Sci. Part B Polym. Phys. 40 (2002) 1673–1681.

[41] I.M. Kalogeras, W. Brostow, Glass transition temperatures in binary polymer blends, J. Polym. Sci. Part B Polym. Phys. 47 (n.d.) 80–95. doi:10.1002/polb.21616.

[42] Z. Qiu, S. Fujinami, M. Komura, K. Nakajima, T. Ikehara, T. Nishi, Nonisothermal crystallization kinetics of poly (butylene succinate) and poly (ethylene succinate), Polym. J. 36 (2004) 642.

[43] M.-L. Xue, J. Sheng, Y.-L. Yu, H.H. Chuah, Nonisothermal crystallization kinetics and spherulite morphology of poly(trimethylene terephthalate), Eur. Polym. J. 40 (2004) 811–818. doi:10.1016/j.eurpolymj.2003.12.009.

[44] L. Gunaratne, R.A. Shanks, Melting and thermal history of poly (hydroxybutyrate-co-hydroxyvalerate) using step-scan DSC, Thermochim. Acta. 430 (2005) 183–190.

[45] G.J.M. de Koning, P.J. Lemstra, Crystallization phenomena in bacterial poly[(R)-3-hydroxybutyrate]: 2. Embrittlement and rejuvenation, Polymer. 34 (1993) 4089–4094. doi:10.1016/0032-3861(93)90671-V.

[46] R. Crétois, J.-M. Chenal, N. Sheibat-Othman, A. Monnier, C. Martin, O. Astruz, R. Kurusu, N.R. Demarquette, Physical explanations about the improvement of PolyHydroxyButyrate ductility: Hidden effect of plasticizer on physical ageing, Polymer. 102 (2016) 176–182. doi:10.1016/j.polymer.2016.09.017.

[47] M.L. Di Lorenzo, P. Sajkiewicz, A. Gradys, P. La Pietra, Optimization of melting conditions for the analysis of crystallization kinetics of poly (3-hydroxybutyrate), E-Polym. 9 (2009).

[48] T. Wang, H. Wang, H. Li, Z. Gan, S. Yan, Banded spherulitic structures of poly(ethylene adipate), poly(butylene succinate) and in their blends, Phys. Chem. Chem. Phys. 11 (2009) 1619–1627. doi:10.1039/B817597G.

[49] B. Wunderlich, Macromolecular Physics, Elsevier, 2012.

[50] T. Liu, Z. Mo, S. Wang, H. Zhang, Nonisothermal melt and cold crystallization kinetics of poly(aryl ether ether ketone ketone), Polym. Eng. Sci. 37 (1997) 568–575. doi:10.1002/pen.11700.

[51] U.W. Gedde, Polymer Physics, Springer Science & Business Media, 2013.

[52] Y.P. Khanna, T.J. Taylor, Comments and recommendations on the use of the Avrami equation for physico-chemical kinetics, Polym. Eng. Sci. 28 (1988) 1042–1045. doi:10.1002/pen.760281605.

[53] G.C. Alfonso, T.P. Russell, Kinetics of crystallization in semicrystalline/amorphous polymer mixtures, Macromolecules. 19 (1986) 1143–1152.

[54] S. Talibuddin, L. Wu, J. Runt, J.S. Lin, Microstructure of melt-miscible, semicrystalline polymer blends, Macromolecules. 29 (1996) 7527–7535.

[55] D. Debier, A.M. Jonas, R. Legras, Blends of polycarbonate and acrylic polymers: Crystallization of polycarbonate, J. Polym. Sci. Part B Polym. Phys. 36 (1998) 2197–2210.

[56] H.D. Keith, F.J. Padden, A Phenomenological Theory of Spherulitic Crystallization, J. Appl. Phys. 34 (1963) 2409–2421. doi:10.1063/1.1702757.

[57] B. Crist, J.M. Schultz, Polymer spherulites: A critical review, Prog. Polym. Sci. 56 (2016) 1–63. doi:10.1016/j.progpolymsci.2015.11.006.

[58] J. Liu, B.-J. Jungnickel, Crystallization kinetical and morphological peculiarities in binary crystalline/crystalline polymer blends, J. Polym. Sci. Part B Polym. Phys. 45 (2007) 1917–1931. doi:10.1002/polb.21162.

[59] B. Vergara-Porras, J.N. Gracida-Rodríguez, F. Pérez-Guevara, Thermal processing influence on mechanical, thermal, and biodegradation behavior in

poly(β-hydroxybutyrate)/poly(ε-caprolactone) blends: A descriptive model, J. Appl. Polym. Sci. 133 (2016). doi:10.1002/app.43569.

[60] B. Zhu, Y. He, N. Yoshie, N. Asakawa, Y. Inoue, Partial Phase Segregation in Strongly Hydrogen-Bonded and Miscible Blends, Macromolecules. 37 (2004) 3257–3266. doi:10.1021/ma035889t.

[61] H.-L. Chen, M.-S. Hsiao, Morphological structure induced by combined crystallization and liquid- liquid demixing in poly (ethylene terephthalate)/poly (ether imide) blends, Macromolecules. 31 (1998) 6579–6584.

[62] S. Nojima, Y. Terashima, T. Ashida, Small-angle X-ray scattering study of the morphology of blends of poly(ε-caprolactone) and polystyrene oligomer, Polymer. 27 (1986) 1007–1013. doi:10.1016/0032-3861(86)90064-9.

[63] S. Nojima, K. Satoh, T. Ashida, Morphology formation by combined effect of crystallization and phase separation in a binary blend of poly (iε-caprolactone) and polystyrene oligomer, Macromolecules. 24 (1991) 942–947.

[64] R.S. Kurusu, N.R. Demarquette, C. Gauthier, J.-M. Chenal, Effect of ageing and annealing on the mechanical behaviour and biodegradability of a poly(3-hydroxybutyrate) and poly(ethylene- *co* -methyl-acrylate- *co* -glycidyl-methacrylate)blend: Mechanical behaviour of PHB/PEMAGMA blends, Polym. Int. 63 (2014) 1085–1093. doi:10.1002/pi.4616.

[65] P.J. Barham, A. Keller, E.L. Otun, P.A. Holmes, Crystallization and morphology of a bacterial thermoplastic: poly-3-hydroxybutyrate, J. Mater. Sci. 19 (1984) 2781–2794. doi:10.1007/BF01026954.

[66] F.B. Khambatta, F. Warner, T. Russell, R.S. Stein, Small-angle x-ray and light scattering studies of the morphology of blends of poly (ϵ-caprolactone) with poly (vinyl chloride), J. Polym. Sci. Polym. Phys. Ed. 14 (1976) 1391–1424.

[67] H. Tanaka, T. Nishi, New types of phase separation behavior during the crystallization process in polymer blends with phase diagram, Phys. Rev. Lett. 55 (1985) 1102.

[68] W. Hu, V.B.F. Mathot, Liquid–liquid demixing in a binary polymer blend driven solely by the component-selective crystallizability, J. Chem. Phys. 119 (2003) 10953–10957. doi:10.1063/1.1619935.

[69] H. Fang, Y. Zhang, J. Bai, Z. Wang, Shear-Induced Nucleation and Morphological Evolution for Bimodal Long Chain Branched Polylactide, Macromolecules. 46 (2013) 6555–6565. doi:10.1021/ma4012126.

[70] N.V. Pogodina, H.H. Winter, S. Srinivas, Strain effects on physical gelation of crystallizing isotactic polypropylene, J. Polym. Sci. Part B Polym. Phys. 37 (1999) 3512–3519. doi:10.1002/(SICI)1099-0488(19991215)37:24<3512::AID-POLB12>3.0.CO;2-#.

[71] K. Boutahar, C. Carrot, J. Guillet, Crystallization of Polyolefins from Rheological MeasurementssRelation between the Transformed Fraction and the Dynamic Moduli, (n.d.).

[72] E. Di Maio, S. Iannace, L. Sorrentino, L. Nicolais, Isothermal crystallization in PCL/clay nanocomposites investigated with thermal and rheometric methods, Polymer. 45 (2004) 8893–8900. doi:10.1016/j.polymer.2004.10.037.

[73] J.F. Vega, D.G. Hristova, G.W.M. Peters, Flow-induced crystallization regimes and rheology of isotactic polypropylene: Effects of molecular architecture, J. Therm. Anal. Calorim. 98 (2009) 655–666. doi:10.1007/s10973-009-0516-3.

[74] J. Shen, L. Ye, K. Xie, Z. Li, Q. Jiao, Z. Chen, Y. Li, Unexpected brittleness: Does the major component in binary polymer blends always make sense?, Polymer. 142 (2018) 218–225. doi:10.1016/j.polymer.2018.03.035.

[75] A. Siegmann, Crystallization of crystalline/crystalline blends: Polypropylene/polybutene-1, J. Appl. Polym. Sci. 27 (1982) 1053–1065. doi:10.1002/app.1982.070270324.

[76] L.A. Utracki, ed., Polymer Blends Handbook, Springer Netherlands, Dordrecht, 2003. doi:10.1007/0-306-48244-4.

[77] A. El-Hadi, R. Schnabel, E. Straube, G. Müller, S. Henning, Correlation between degree of crystallinity, morphology, glass temperature, mechanical properties and biodegradation of poly (3-hydroxyalkanoate) PHAs and their blends, Polym. Test. 21 (2002) 665–674. doi:10.1016/S0142-9418(01)00142-8.

[78] A.J. Kinloch, Fracture Behaviour of Polymers, Springer Science & Business Media, 2013.

[79] H.-H. Kausch, Polymer Fracture, Springer Science & Business Media, 2012.

[80] G.J.M. de Koning, A.H.C. Scheeren, P.J. Lemstra, M. Peeters, H. Reynaers, Crystallization phenomena in bacterial poly[(R)-3-hydroxybutyrate]: 3. Toughening via texture changes, Polymer. 35 (1994) 4598–4605. doi:10.1016/0032-3861(94)90809-5.

Appendix A. Supplementary material

T_g deviations from linearity

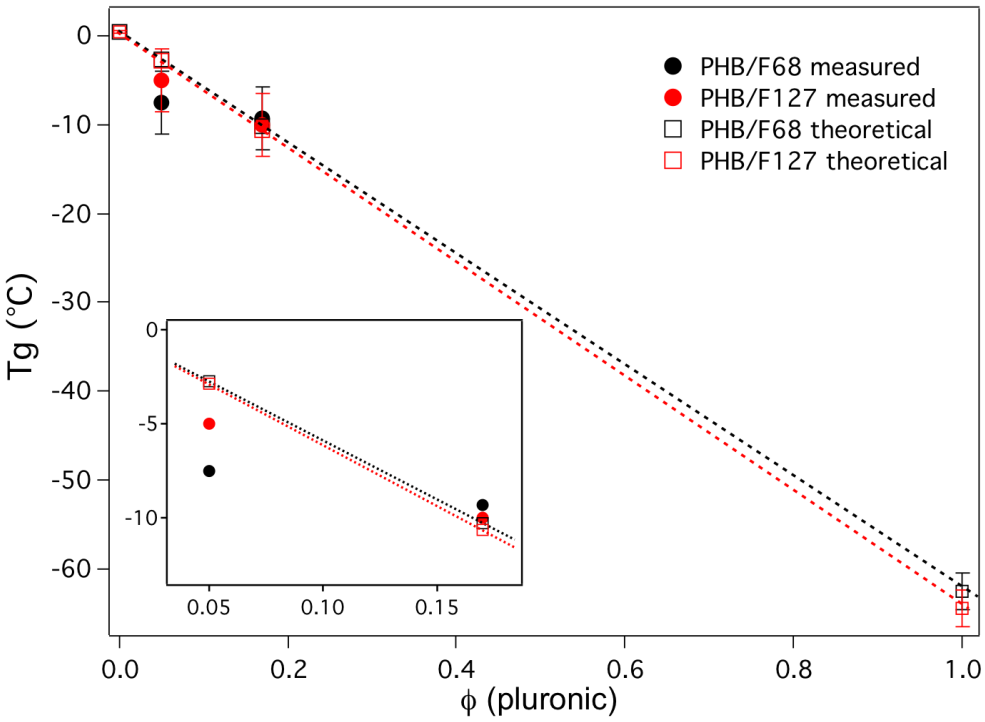

Figure S1. Plot of the measured and theoretical T_g values for the investigated PHB/pluronics blends.

Presence of crystalline pluronic in the as-prepared F127-17 blend

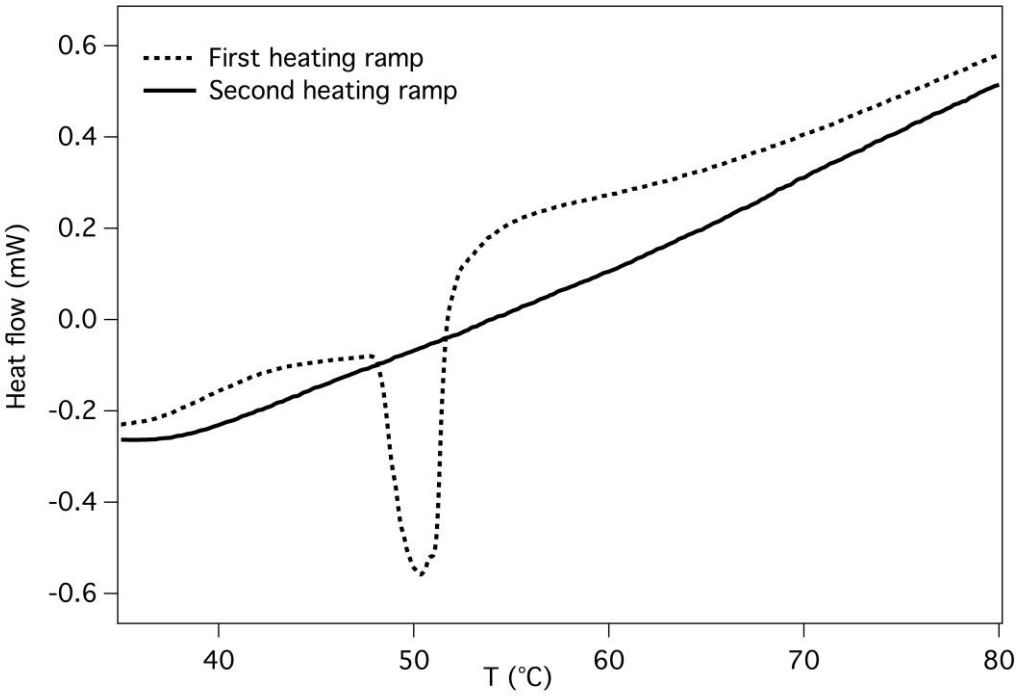

Figure S2. DSC profile of F127-17 blend showing the presence of crystalline pluronic in the first heating ramp (dotted line).

SAXS curves on the as-prepared films

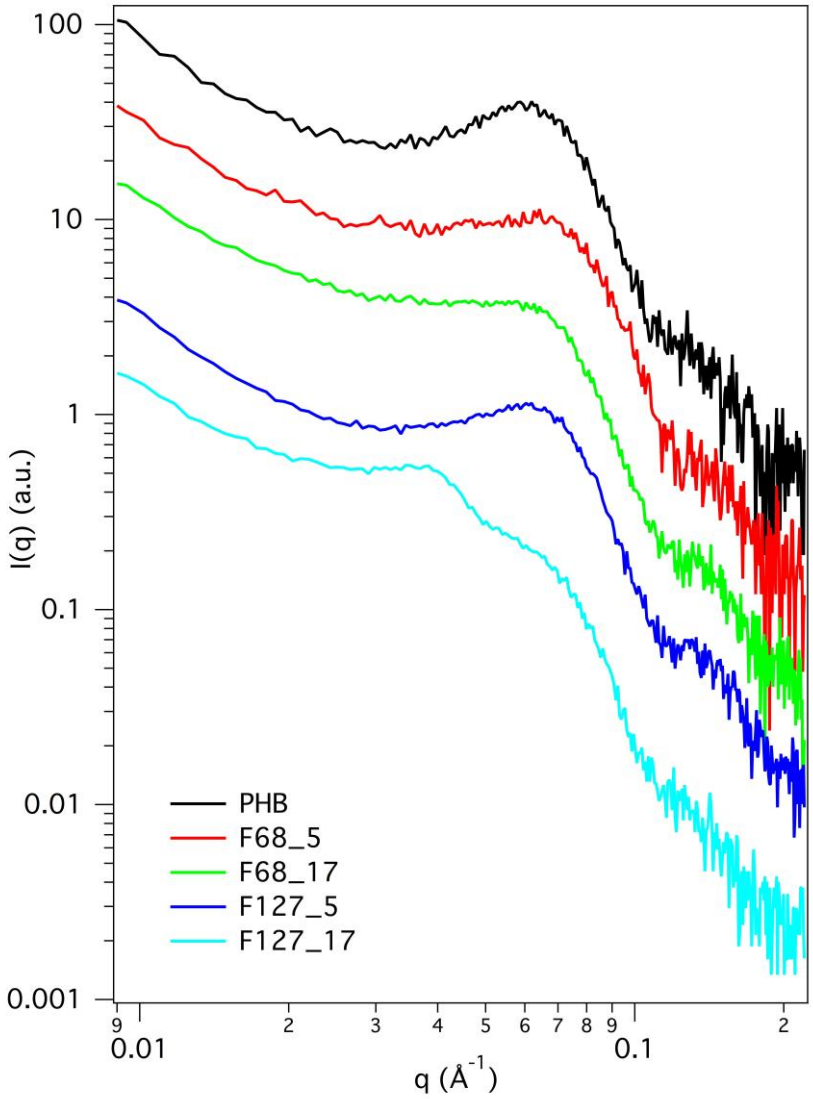

Figure S3. SAXS profiles for neat PHB and all PHB/pluronics blends. All curves are offset along y-axis.

1D-correlation function obtained from SAXS curves

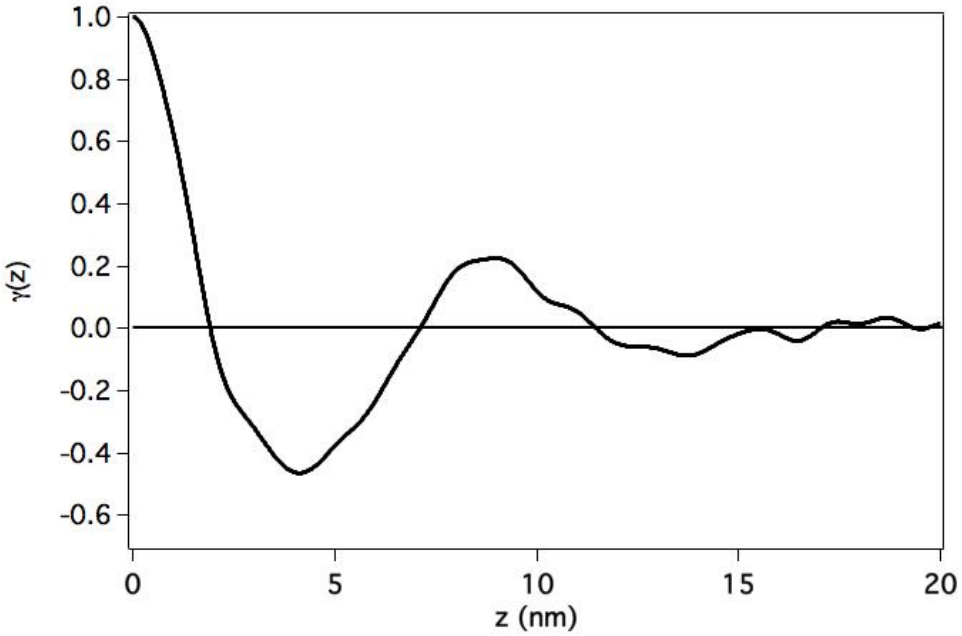

Figure S4. 1D-correlation function for the as-prepared neat PHB film.

Comparison between the crystallization half-times obtained from DSC and rheology measurements

Table S1. Values of crystallization half-time taken as the time necessary to reach a relative crystallinity value equal to 0.5 as obtained from DSC ($t_{1/2\mathrm{DSC}}$) and rheology ($t_{1/2\mathrm{rheo}}$) for all the investigated samples.

Sample	$t_{1/2\mathrm{DSC}}$ (min)	$t_{1/2\mathrm{rheo}}$ (min)
PHB	24.63	13.56
F68-5	25.35	13.38
F68-17	26.67	13.69
F127-5	25.97	13.30
F127-17	27.30	13.88